Analysis of Turbulent Underexpanded Jets, Part I: Parabolized Navier-Stokes Model, SCIPVIS

S. M. Dash* and D. E. Wolf†
Science Applications Inc., Princeton, New Jersey
and
J. M. Seiner‡
NASA Langley Research Center, Hampton, Virginia

A new computational model, SCIPVIS, is described, which predicts the multiple-cell wave/shock structure in under- or overexpanded turbulent jets. SCIPVIS solves the parabolized Navier-Stokes jet mixing equations utilizing a shock-capturing approach in supersonic regions of the jet and a pressure-split approach in subsonic regions. Turbulence processes are represented by the solution of compressibility corrected two-equation turbulence models. SCIPVIS presently analyzes jets exhausting into a quiescent or supersonic external stream for which a single-pass spatial marching solution can be obtained. The features of SCIPVIS are reviewed and calculations are described exhibiting the influence of turbulence modeling, jet temperature, and flight velocity on the jet shock structure. A detailed assessment of SCIPVIS via comparisons with laboratory data and its implementation in jet shock-noise studies is provided in Part II of this article.

I. Introduction

THE ability to predict the acoustic characteristics of an underexpanded turbulent jet (Fig. 1) is contingent upon representing the mean flow and turbulence structure in a detailed and realistic fashion. Previous studies[1-3] have highlighted the strongly interactive aspects of the jet flow structure problem and the inadequacy of inviscid modeling techniques to represent the wave/shock structure beyond the jet near field (i.e., first several shock cells). The prediction of the detailed multiple shock-cell flow structure entails the strongly interactive coupling of wave and turbulent mixing processes, and the appropriate representation of turbulence processes in the highly compressible environment occurring in underexpanded jets. While a number of underexpanded turbulent jet models have been developed which treat several of the above processes (see Ref. 3), none provide for the generalized analysis of the multiple-cell wave/turbulent structure over a significant range of operational conditions.

A new parabolized Navier-Stokes model, SCIPVIS, has been developed which analyzes the above processes in a detailed fashion. SCIPVIS solves a fully coupled system of viscous/inviscid equations which intimately relates the effect of turbulent mixing processes on the wave structure, and employs specialized techniques to treat various aspects of the strongly interactive processes occurring in the jet.[3] The development of SCIPVIS was prompted by requirements in a number of problem areas as discussed in Refs. 3 and 4. This paper will discuss aspects of the SCIPVIS model relevant to the jet shock-noise problem area. The features and capabilities of SCIPVIS in analyzing the multiple-cell wave structure in turbulent jets will be presented and pertinent computational procedures relevant to achieving these capabilities will be highlighted. In Part II of this paper, the performance of the SCIPVIS model is assessed via comparisons with laboratory data for a series of over- and underexpanded jets; and, its implementation in the prediction of jet shock noise is delineated.

Presented as part of Paper 83-0704 at AIAA 8th Aeroacoustics Conference, Atlanta, Ga., April 11-13, 1983; received May 18, 1983; revision received May 23, 1984.

*Technical Director, Propulsion Gas Dynamics Division. Member AIAA.
†Research Scientist, Propulsion Gas Dynamics Division. Member AIAA.
‡Research Engineer, Aeroacoustics Branch, Acoustics and Noise Reduction Division. Member AIAA.

II. Overview of Modeling Techniques in SCIPVIS

SCIPVIS incorporates technology formulated over the past several years in programs geared to the viscous/inviscid analysis of rocket and aircraft exhaust plumes.[5-8] The treatment of wave/shock processes in inviscid flow regions is performed utilizing the SCIPPY model shock-capturing approach of Dash and Thorpe.[9] The extension of this shock-capturing approach to supersonic viscous flow regions involves the addition of parabolized stress-transport terms which render the resulting viscous/inviscid jet equations hyperbolic/parabolic. The shock-capturing algorithm utilized in SCIPVIS is described in Refs. 3 and 10. In earlier papers,[3,4] the ability of this shock-capturing algorithm to analyze basic interactive phenomena occurring in supersonic mixing regions was demonstrated (e.g., the interaction of expansion fans and shock waves with shear layers, waves generated by high Mach turbulent dissipative processes, etc.), and complete jet flowfield solutions were generated.

Turbulence phenomena in SCIPVIS are represented using conventional models of the two-equation class which solve partial differential equations for the variation of the turbulent kinetic energy and length scale parameter. This level of turbulence modeling represents the present state-of-the-art for jet flowfields.[11] Applications to a complete spectrum of simple (constant pressure) free-jet problems[12] had indicated that basic two-equation turbulence models performed reliably for low-speed jet problems but not for supersonic jet problems. Present-generation two-equation models are all formulated from an incompressible viewpoint and, thus, their inability to deal with compressible phenomena is not surprising. Extensions of two-equation models to deal with compressibility effects thus far have been heuristically formulated[11,13] (viz., no attempt has yet been made to formally model the terms embodying the compressibility effects of high Mach numbers). A detailed assessment of the performance of compressibility modified two-equation turbulence models for both simple and

complex (variable pressure, chemically reacting) jet flowfields is given in Ref. 11. An overview of high Mach number compressibility effects on turbulent mixing and the specific "compressibility corrected" turbulence models employed in SCIPVIS will be presented. No attempt has been made in the present effort to model the large-scale structure of the turbulence associated with the acoustic excitation of jet instability modes.

The strongly interactive coupling of the viscous/inviscid jet solution with an Euler or potential external flow solution is performed using a direct-coupling technique. The coupling of the jet and external flow solutions is performed at the outer edge of the jet mixing layer boundary (viz., at the turbulent/nonturbulent interface). For supersonic external flows, the complete jet/external flow calculation is performed in a single sweep in view of the hyperbolic/parabolic characteristics of the governing equations. For quiescent external flow, the ambient pressure is imposed as the outer boundary pressure and a single sweep calculation can also be performed. For subsonic external flows, the streamwise pressure variation determined by a potential flow solution would be imposed as the jet outer pressure. The external potential flow is solved using an injection boundary condition along the jet outer viscous boundary based on the entrainment velocity determined in the viscous/inviscid jet solution. Arrival at a converged flowfield solution entails several iterations between the viscous/inviscid jet and potential flow solutions; the iterative methodology parallels that developed by Wilmoth and Dash[14] utilizing overlaid viscous/inviscid coupling.[15] The present version of SCIPVIS is operational for quiescent or supersonic external flows, as will be described. Extensions for the iterative coupling with a subsonic/transonic potential flow solver are now in progress, as described in Ref. 10.

In analyzing jets with a quiescent or subsonic external stream, a formal matching procedure is required at the viscous sonic line (Fig. 1), and specialized techniques are required to permit spatial marching in subsonic portions of the flow. Subsonic/supersonic coupling is performed utilizing the viscous-characteristic approach introduced by Ferri and Dash[16] for sonic line matching in the interactive analysis of supersonic boundary layers. Spatial marching in subsonic regions is accomplished utilizing pressure-splitting techniques[17] which decouple the streamwise and normal pressure gradients. The streamwise gradient is *imposed* (i.e., set equal to the external pressure variation) rendering the subsonic equations parabolic rather than elliptic. Normal pressure variations are obtained via a coupled solution of the continuity and normal momentum equations subject to the imposed outer pressure variation and the viscous-characteristic pressure/flow deflection constraint at the sonic line.

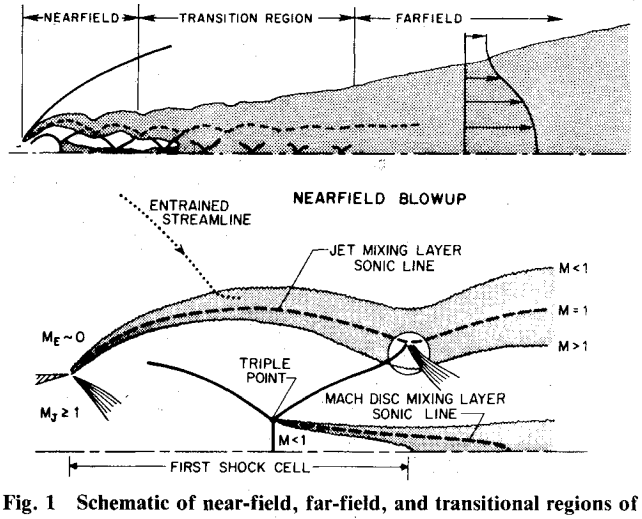

Fig. 1 Schematic of near-field, far-field, and transitional regions of turbulent underexpanded jets.

SCIPVIS contains provisions for treating both regular and Mach disk type shock reflections using the triple-point methodology described in Ref. 9. In situations with Mach disks, the turbulent mixing occurring along the Mach disk slipstream (Fig. 1) induces significant downward deflections of the adjacent flow due to the wake-like characteristics of the mixing process.[3] This is accounted for utilizing the subsonic/supersonic sonic line coupling discussed previously and a variant of the pressure-split procedure employing a sublayer-type approximation[3,10] to suppress elliptic upstream influence effects (viz., departure solutions).

III. Governing Equations

Conservative Form of Mean Flow Equations

The time-averaged, Reynolds decomposed equations governing the planar ($J=0$) or axisymmetric ($J=1$) flow in a moderately under- or overexpanded jet[10] are listed below.

Continuity:

$$\frac{\partial}{\partial x}(\rho U r^J)+\frac{\partial}{\partial r}(\rho V r^J)=0 \tag{1}$$

Streamwise (axial) momentum:

$$\frac{\partial}{\partial x}([P+\rho U^2]r^J)+\frac{\partial}{\partial r}(\rho UV r^J)=\frac{\partial}{\partial r}\left(r^J\left[\mu\frac{\partial U}{\partial r}-\rho\overline{u'v'}\right]\right) \tag{2}$$

Normal (radial) momentum:

$$\frac{\partial}{\partial x}(\rho V r^J)+\frac{\partial}{\partial r}([P+\rho V^2]r^J)=0 \tag{3}$$

Energy:

$$\frac{\partial}{\partial x}(\rho UH r^J)+\frac{\partial}{\partial r}(\rho VH r^J)=\frac{\partial}{\partial r}\left(r^J\left[\mu\frac{\partial H}{\partial r}-\rho\overline{H'v'}\right]\right) \tag{4}$$

Species continuity:

$$\frac{\partial}{\partial x}(\rho U\phi r^J)+\frac{\partial}{\partial r}(\rho V\phi r^J)=\frac{\partial}{\partial r}\left(r^J\left[\mu\frac{\partial \phi}{\partial r}-\rho\overline{\phi'v'}\right]\right) \tag{5}$$

These equations have been parabolized with respect to the axial (x) direction (viz., all stress/diffusive terms with axial derivatives have been deleted) and "standard" (incompressible) assumptions concerning the turbulence correlations have been invoked [viz., third- and higher-order correlations, density correlations ($\rho'u'$, ρ', H', and $\rho'\phi'$), and all correlation terms in the normal momentum equation are neglected]. For simplicity in describing the equations, the extra terms associated with nonunity values of the Prandtl numbers, σ have not been listed above (these terms are incorporated in SCIPVIS and will be given below in their final form). In the above equations, U and V are the axial and radial velocity components, ρ the density, P the pressure, μ the laminar viscosity, H the total enthalpy, and ϕ the species parameter defined by

$$\boxed{\phi=\frac{\alpha_i-\alpha_{i_E}}{\alpha_{i_J}-\alpha_{i_E}}} \tag{6}$$

where α_i is the mass fraction of the ith species and J and E designate the constant values of α_i in the unmixed jet and external streams. The composition in both unmixed streams is taken to be uniform and the chemistry is taken to be frozen.

Turbulent Transport Terms

Classical Boussinesq-type approximations are utilized in representing the turbulent shear stress and scalar transport terms. Thus

$$-\rho\overline{u'v'} = \mu_t \frac{\partial U}{\partial r} \tag{7a}$$

$$-\rho\overline{H'v'} = \frac{\mu_t}{\sigma_H}\frac{\partial H}{\partial r} \tag{7b}$$

$$-\rho\overline{\phi'v'} = \frac{\mu_t}{\sigma_\phi}\frac{\partial \phi}{\partial r} \tag{7c}$$

where μ_t is the turbulent viscosity and σ_H and σ_ϕ the effective turbulent Prandtl numbers for the transport of energy and species.

Two-Equation Turbulence Models

In the generalized Prandtl-Kolmogoroff turbulence formulation (see, e.g., Ref. 18) the turbulent viscosity μ_t is related to the turbulent kinetic energy k and turbulent length scale ℓ, via

$$\mu_t = C_\mu \rho k^{1/2} \ell \tag{8}$$

where C_μ is a dimensionless constant. A partial differential equation can be formally derived to describe the production, dissipation, and transport of turbulent kinetic energy. By analogy,[18] an equation can be formulated for the length scale parameter z, which is related to k and ℓ by

$$z = k^m \ell^n \tag{9}$$

Table 1 shows three different popular forms of the length scale equation. Only the $k\epsilon$ and kW two-equation models have been incorporated in SCIPVIS. The $k\omega$ model of Ref. 20 (in particular, the modified version which accounts for compressibility[21]) does show promise, as demonstrated by Walker[22] in his evaluation against Mach 2.2 jet data. However, this model has not been assessed against a significant body of compressible jet data.

$k\epsilon$ Turbulence Model

The $k\epsilon 2$ model[12] incorporated in SCIPVIS is an extended form of the $k\epsilon$ model which contains both axisymmetric and weak shear flow "corrections." The turbulent viscosity μ_t is determined from the local values of k and ϵ via the relation

$$\mu_t = C_\mu(f,g)\rho(k^2/\epsilon) \tag{10}$$

The following model constants[12] are utilized in SCIPVIS:

$$\sigma_k = 1.0, \quad \sigma_\epsilon = 1.3, \quad C_1 = 1.4$$

$$C_2 = 1.94 - 0.1336f, \quad C_\mu = 0.09\, g(\overline{P/\epsilon}) - 0.0534f$$

The axisymmetric correction parameter f is set equal to zero in the shear-layer region (before the mixing zone reaches the axis), and is defined by

$$f = \left[\frac{r_e}{2(u_c - u_e)}\left(\left|\frac{du_c}{dx}\right| - \frac{du_c}{dx}\right)\right]^{0.2} \tag{11}$$

Table 1 Forms of the length scale equation

Model	z	m	n	$\mu_t/C_\mu\rho$
$k\epsilon$ (Ref. 12)	ϵ	3/2	−1	k^2/ϵ
kW (Ref. 19)	W	1	−2	$k/W^{1/2}$
$k\omega$ (Ref. 20)	ω	1/2	−1	k/ω

downstream of that point (r_e is the width of the full mixing layer, u_c the jet centerline velocity, and u_e the external stream velocity). The weak shear flow correction g is a function of the shear-stress weighted average ratio of production to dissipation rates. The functional form of $g(\overline{P/\epsilon})$ is given in Ref. 12.

Compressibility Corrected Version of $k\epsilon$ Model ($k\epsilon 2$,cc)

The performance of the $k\epsilon$ model in analyzing supersonic jet and shear-layer data has been shown to be quite poor.[12] An effort was undertaken to correct this model in a heuristic fashion[13] to account for the reduced mixing rates observed for higher Mach number jet mixing. The compressibility corrected viscosity is given by

$$\mu_t = K(M_\tau) C_\mu \rho (k^2/\epsilon) \tag{12}$$

where $K(M_\tau)$ is the correction factor and M_τ the characteristic Mach number of turbulence ($M_\tau = \sqrt{k_{\max}}/a$, where $k_{\max}$ is the maximum value of k at each station and a the local sound speed at the grid point where k is maximum). The functional form of $K(M_\tau)$, given in Fig. 2, was determined by matching calculations to observed spread rates for isoenergetic, supersonic shear layers with one stream stationary.[23] Figure 2 exhibits the performance of the $k\epsilon 2$ and $k\epsilon 2$,cc models in predicting this spread rate data; the $k\epsilon 2$ model shows no variation with Mach number while the $k\epsilon 2$,cc model duplicates the data [per calibration of $K(M_\tau)$]. Note that the compressibility correction term goes to unity as compressibility effects diminish and, hence, the $k\epsilon 2$ and $k\epsilon 2$,cc models are equivalent in lower speed situations.

***kW* Turbulence Model**

The kW model,[19] although developed at about the same time as the $k\epsilon$ model, has not been widely used due to complications in applying it to wall-bounded shear flows.[24] However, a version of the kW model[25] with coefficients set by

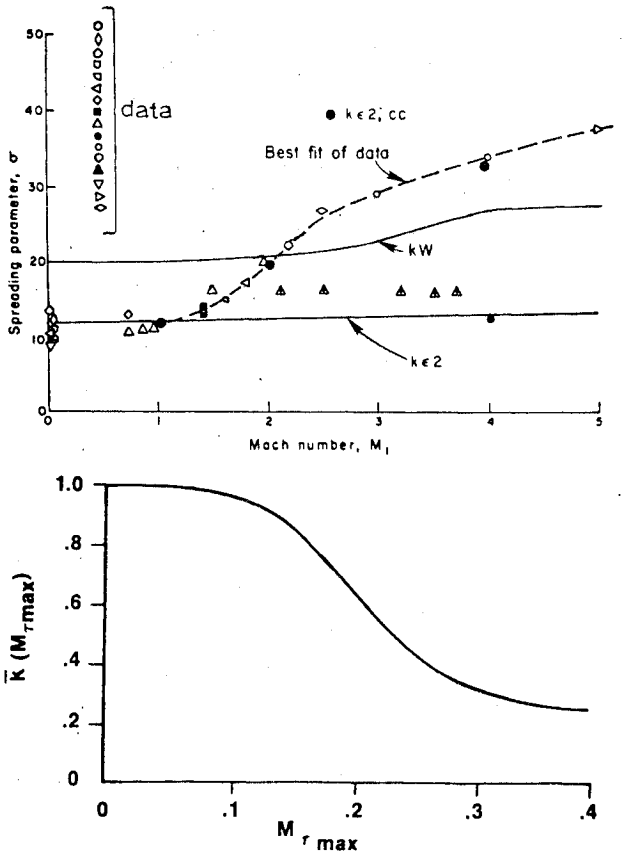

Fig. 2 Variation of spread parameter σ with Mach number and compressibility correction factor for $k\epsilon 2$ turbulence model.

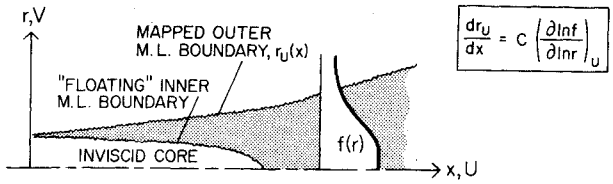

Fig. 3a SCIPVIS parabolic (turbulent mixing) operational mode.

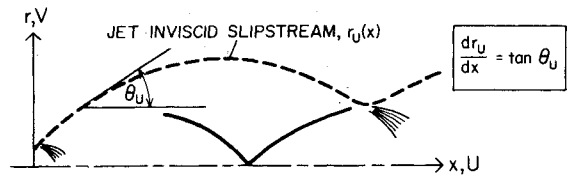

Fig. 3b SCIPVIS hyperbolic (supersonic wave) operational mode.

rocket plume data has been employed successfully by the Propellant and Rocket Motor Establishment (PERME) in Great Britain. Predictions by PERME simulating laboratory rocket plume experiments performed at Arnold Engineering Development Center[26] were quite promising and the overall assessment of this model by Pergament[11] for a spectrum of jet mixing problems was favorable. Hence, this model has been incorporated into SCIPVIS.

The turbulent viscosity is given by

$$\mu_t = \rho k / W^{1/2} \tag{13}$$

and the following model constants[25] are utilized:

$$\sigma_k = 0.86, \quad \sigma_\epsilon = 0.86, \quad C_D = 0.09$$

$$C_1 = 1.48, \quad C_2 = 0.18, \quad C_3 = 3.5$$

Note that this model contains no axisymmetric or weak shear flow correction terms.

Mapped, Vectorized Conservation Equations

The conservative system of mean flow and turbulence model equations is solved in a mapped coordinate system (to be described in Sec. IV) utilizing the simple rectangular transformation.

$$\boxed{\begin{aligned} \xi &= x \\ \eta &= (r - r_L(x))/(r_U(x) - r_L(x)) \end{aligned}} \tag{14}$$

where r_L and r_U are the boundaries of the jet domain being solved. With this transformation, the equations can be expressed in the following vector form:

$$\boxed{\frac{\partial \bar{E}}{\partial \xi} + \frac{\partial \bar{F}}{\partial \eta} = \frac{b^2}{r^J}\frac{\partial}{\partial \eta}\left(\frac{r^J \mu_{\text{eff}}}{\sigma_f}\frac{\partial \bar{f}}{\partial \eta}\right) + \bar{G}_f} \tag{15}$$

where

$$\bar{f} = [1,\ U,\ V,\ H,\ \phi,\ k^{(1)},\ \epsilon,\ k^{(2)},\ W]^T$$

Here (1) designates the $k\epsilon$ model, and (2) the kW model.

$$\bar{E} = \begin{bmatrix} e_\rho \\ e_U \\ e_V \\ e_H \\ e_\phi \\ e_k^{(1)} \\ e_\epsilon \\ \hline e_k^{(2)} \\ e_W \end{bmatrix} = \begin{bmatrix} \rho U \\ \alpha P + \rho U^2 \\ \rho UV \\ \rho UH \\ \rho U\phi \\ \rho Uk^{(1)} \\ \rho U\epsilon \\ \hline \rho Uk^{(2)} \\ \rho UW \end{bmatrix}; \quad \bar{F} = b \underbrace{\begin{bmatrix} \rho V \\ \rho UV \\ P + \rho V^2 \\ \rho VH \\ \rho V\phi \\ \rho Vk^{(1)} \\ \rho V\epsilon \\ \hline \rho Vk^{(2)} \\ \rho VW \end{bmatrix}}_{\bar{F}} - a\bar{E}$$

and

$$\bar{G}_f = \begin{bmatrix} 0 \\ (\alpha - 1)\overline{\partial P/\partial x} \\ 0 \\ \dfrac{b^2}{r^J}\dfrac{\partial}{\partial r}\left(\dfrac{r^J \mu_{\text{eff}}(\sigma_H - 1)}{\sigma_H}\dfrac{\partial}{\partial r}\left(\dfrac{U^2}{2}\right)\right) \\ 0 \\ \underline{P} - \epsilon \\ (C_1\underline{P} - C_2\rho\epsilon)\epsilon/k \\ \hline \underline{P} - \rho C_D k W^{1/2} \\ \dfrac{C_1 W\underline{P} - C_2\rho k W^{3/2}}{k} + C_3\mu_t\left(\dfrac{\partial^2 U}{\partial r^2}\right)^2 \end{bmatrix} - a_\eta \bar{E} - (J/r)\bar{F}$$

In the above equations, a and b are the transformation parameters given by

$$a(\xi,\eta) = [(1-\eta)r_L' + \eta r_U']/(r_U - r_L)$$

$$b(\xi) = 1/(r_U - r_L) \tag{16}$$

$\underline{P}$ is the turbulent production term [i.e., $\underline{P} = \mu_t(\partial U/\partial r)^2$], and α a flow indicator ($\alpha = 1$ for supersonic flow regions, 0 for subsonic flow regions). The variable μ_{eff} is the combined laminar and turbulent viscosity. Boundary points and subsonic/supersonic matching points are analyzed using viscous-characteristic equations[16] whose description is given in Refs. 3 and 10.

IV. Computational Features of SCIPVIS

Integration Options

SCIPVIS provides for the spatial integration of the viscous/inviscid jet equations [Eq. (15)] using four types of integration options which are summarized below.

1. Parabolic (Constant Pressure Mixing) Option

This option is utilized to analyze constant pressure subsonic or supersonic jets. In utilizing this option the parameter α in Eq. (15) is set equal to zero (which removes the pressure term from the streamwise momentum conservation variable, e_U); the normal momentum equation is eliminated; the streamwise pressure gradient term $\partial P/\partial X$ in the $\bar{G}_f$ vector array is set equal to zero; and, a parabolic decode procedure[3,10] is used to extract the mean flow variables U, H, and ϕ from the $\bar{E}$ conservation variables e_U, e_H, and e_ϕ. In analyzing a balanced pressure jet (Fig. 3a), the equations are mapped from the jet axis to the outer edge of the jet mixing layer, $r_U(X)$, along which the external flow conditions U_E, H_E, and $\phi = 0$ are prescribed. The inner mixing layer boundary "floats" across the grid points until it reaches the axis. The parabolic boundary growth rate dr_U/dX is based on the edge gradients of

streamwise velocity U and species parameter ϕ, and is given by

$$\left.\frac{dr_U}{dx}\right|_{vis} = \frac{Cr_U}{f_L}\left(\frac{\partial f}{\partial r}\right)_U \tag{17}$$

where f represents U and ϕ (the maximum gradient is utilized) and a value of $C \sim 1$ places the computational boundary r_U in close proximity with the physical mixing layer boundary (increasing C yields a buffer region of nonturbulent flow between the physical mixing layer edge and r_U but does not affect the calculation except for decreasing the grid resolution). This option is also employed for underexpanded jets exhausting into quiescent or subsonic streams for analyzing the subsonic portion of the jet mixing layer, as will be described below.

2. Partially Parabolic Option

This is an extension of the above option to account for normal pressure variations across the subsonic portion of the jet mixing layer using a pressure-splitting approximation.[17] Here, the preceding parabolic option is first exercised (in integrating the equations from X to $X+\Delta X$) with the streamwise pressure gradient term $\partial P/\partial X$ set equal to the outer-edge pressure gradient. This yields the flow variables U, H, and ϕ at $X+\Delta X$.

The pressure, density, and radial velocity variation across the mixing layer are then arrived at via the coupled integration of the continuity and normal momentum equations and the equation of state constraint. The details of the cross-flow integration are given in Ref. 10. A new, noniterative cross-flow integration procedure developed by Dash and Sinha[27] for curved wall jet flows is presently being incorporated into SCIPVIS.

3. Hyperbolic (Inviscid Supersonic) Option

This option can be utilized to predict the near-field inviscid wave/shock structure in the jet in weakly interactive situations[3] and, of course, is utilized to predict the inviscid core region of underexpanded jets in all situations. To predict the inviscid supersonic jet structure (Fig. 3b) the diffusive terms are set equal to zero, the turbulence equations are eliminated, and the equations are integrated with the parameter α set equal to one (i.e., the pressure is included in the e_U conservative variable). The inviscid jet equations are mapped from the axis to the jet interface r_U defined by

$$\left.\frac{dr_U}{dx}\right|_{inv} = \tan\theta_U \tag{18}$$

The pressure along the interface r_U is prescribed for quiescent or subsonic external flow and is determined by a concurrent external flow solution (or the use of pressure/flow deflection rules such as shock expansion theory) for supersonic external flows (see Ref. 9). A supersonic decode procedure[9] is used to arrive at the flow variables U, V, P, H, and ϕ.

4. Hyperbolic/Parabolic (Viscous Supersonic) Option

This option is utilized to analyze supersonic viscous (turbulent) regions of the jet. It is a direct extension of the hyperbolic option with the diffusive terms evaluated and the turbulence model equations integrated. Details of the numerical algorithm and the analysis of basic supersonic interactive phenomena are provided in Refs. 3, 4, and 10.

The application of the preceding integration options in analyzing supersonic underexpanded jets exhausting into a supersonic quiescent stream will be discussed below.

Underexpanded Jet/Supersonic External Stream

Referring to Fig. 4, the analysis of this fully supersonic problem (in the absence of embedded subsonic zones behind Mach disks) involves utilization of the hyperbolic and hyperbolic/parabolic integration options. This is accomplished by utilizing the techniques summarized below.

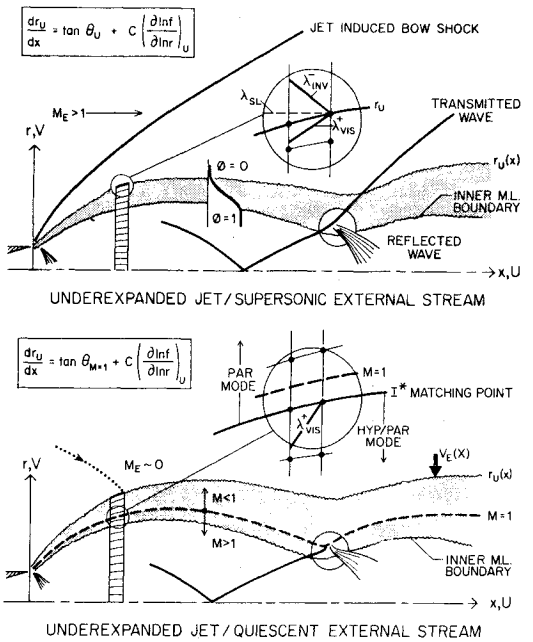

Fig. 4 Operational modes of SCIPVIS for supersonic and quiescent external streams.

1) Grid points are evenly distributed between the jet axis and the outer jet viscous/inviscid boundary, $r_U(X)$.

2) The viscous/inviscid boundary growth is obtained by combining Eqs. (17) and (18) as follows:

$$\left.\frac{dr_U}{dx}\right|_{vis/inv} = \tan\theta_U + \frac{Cr_U}{f_L}\left(\frac{\partial f}{\partial r}\right)_U \tag{19}$$

3) The position of the inner mixing layer boundary which "floats" across the grid points in working its way down to the axis is monitored by inspection of the ϕ profile at each integration step. The hyperbolic (inviscid) equations are integrated below this position while the hyperbolic/parabolic (viscous/inviscid) equations are integrated above this position.

4) Properties along the outer viscous/inviscid boundary $r_U(X)$ are obtained by solving

a) inner (λ^+_{vis}) and outer (λ^-_{inv}) characteristic compatibility relations for the pressure, P_U, and flow angle, θ_U (or an outer pressure/flow deflection relation in lieu of the λ^-_{inv} compatibility relation) and

b) isentropic streamline relations along the entrained streamline λ_{SL} (i.e., $H=H_E$, $P/\rho^\gamma = \text{const}$) to yield remaining flow properties.

The insert to Fig. 4 depicts the details of the boundary-point calculation.

Underexpanded Jet/Quiescent External Stream

Referring to Fig. 4, the analysis of this problem involves utilization of both the hyperbolic and hyperbolic/parabolic integration options required in the fully supersonic problem, plus the parabolic or partially parabolic integration option to analyze the subsonic portion of the jet mixing layer. This is accomplished utilizing the techniques summarized below.

1) Grid points are evenly distributed as above from the jet axis to the outer jet viscous/inviscid boundary, $r_U(X)$.

2) The boundary growth is obtained by combining the viscous growth rule with the flow deflection angle at the sonic line (not the outer edge angle as in the supersonic flow case),

viz.,

$$\left.\frac{dr_U}{dx}\right|_{\text{vis/inv}} = \tan\theta_{M=1} + \frac{Cr_U}{f_L}\left(\frac{\partial f}{\partial r}\right)_U \tag{20}$$

3) As in the fully supersonic case, the position of the "floating" inner mixing layer boundary is used to delineate between hyperbolic and hyperbolic/parabolic flow regions. The hyperbolic/parabolic integration is performed in the region bounded by the inner mixing layer boundary and the jet mixing layer sonic line.

4) Above the sonic line, the equations are integrated using the parabolic option with the streamwise pressure gradient, $\partial P/\partial X$, set equal to zero. The position of the sonic line is monitored at each integration step and also "floats" through the grid points, ultimately reaching the jet axis in the far field at which point all "steady" wave processes terminate.

5) Two options are available to represent the radial variation of pressure and radial velocity across the subsonic portion of the mixing layer which works as follows:

a) Parabolic Option. The pressure variation across the subsonic region is neglected (this is a reasonable approximation for the quiescent problem at modest pressure ratios; it would be a poorer approximation for the near-field jet with a subsonic external flow since the streamline curvature induced by the "washing away" of the mass defect region of the external boundary layer can be quite appreciable (see Refs. 14 and 15). Here, the external pressure is imposed at the subsonic/supersonic matching point (see insert of Fig. 4) yielding the flow deflection angle θ^*, and, hence, all remaining flow properties (since U, H, and ϕ are known from the parabolic solution). Upward integration of the continuity equation yields the radial variation of V and, hence, the edge entrainment (radial) velocity, V_E.

b) Partially Parabolic Option. The pressure P^* is *assumed* at the sonic line yielding θ^* and all remaining flow properties as above. Integration of continuity and normal momentum (see Refs. 3 and 10) yields the radial variation of P and V. The process is iterated upon until the predicted edge pressure is equivalent to the imposed external pressure.

In performing quiescent external stream calculations, imposition of the ambient pressure level along r_U and the use of the boundary condition, $U_E = 0$ (in practice, a nominal value $\sim U_J/100$ is employed) is only a first approximation to the complete interactive problem. The entrainment velocity $V_E(X)$ predicted in this first approximation accelerates the "nominally" quiescent external flow. The entrainment induced pressure $[P_E(X)]$ and streamwise velocity $[U_E(X)]$ variations (obtained via coupling the jet solution with a potential flow solver) are implemented as boundary conditions along r_U for a subsequent jet solution. This jet/potential flow iterative coupling process is analogous to that required for analyzing a subsonic/transonic external stream. The iterative methodology is now under development as discussed in Refs. 3, 5, and 10.

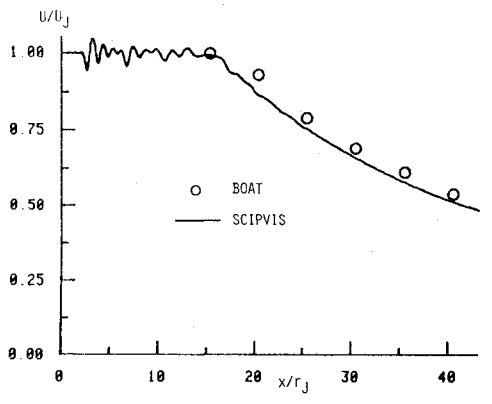

Fig. 5 Comparison of fully coupled SCIPVIS and parabolic BOAT predictions for a balanced pressure Mach 2.2 jet into still air.

Mach Disk Region Analysis

The turbulent mixing that occurs between the inner flow that traverses the disk and the outer flow that traverses the oblique shock system is quite rapid. In fact, for smaller disks, the mixing process dominates the acceleration of the inner flow to supersonic velocities. The mixing process that occurs has wake-like characteristics and the entrainment process induces large negative streamline displacements which can appreciably alter pressure levels from those occurring in the inviscid limit. The treatment of this strongly interactive problem in SCIPVIS utilizes pressure-split methodology whose detailed description is provided in Refs. 3 and 10. Disks are located using the sting triple-point criterion discussed in Ref. 9.

Numerical Algorithm

The generalized two-step (predictor-corrector) numerical algorithm used in various regions of the flow is described in detail in Refs. 3 and 10. Diffusive terms are evaluated using a central difference operator. In supersonic flow regions, the convective terms have been differenced using the MacCormack algorithm.[28] In subsonic flow regions, the convective terms are upwinded. A new variant of the MacCormack algorithm has recently been utilized in supersonic flow regions[3,10] which splits the convective flux operator (for scalar variables only) into upwind and alternating components. This improves the convection of scalar variables in situations where the streamlines and mapped grid lines ($\eta = \text{const}$) are significantly skewed and does not affect the shock-capturing characteristics of the algorithm. Further details of the algorithms, the step sizes, etc., are available in Refs. 3 and 10.

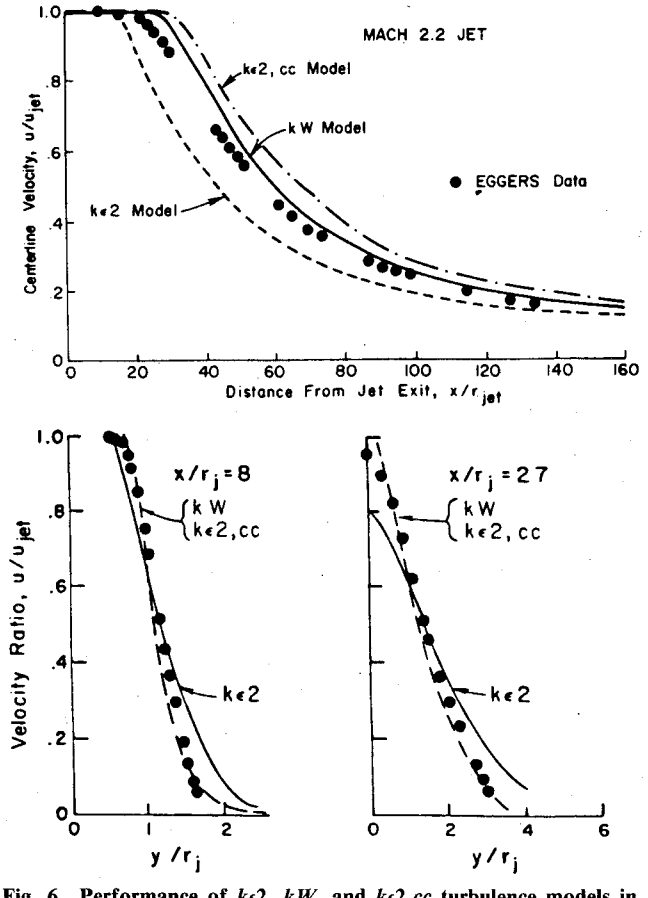

Fig. 6 Performance of $k\epsilon 2$, kW, and $k\epsilon 2,cc$ turbulence models in analyzing Mach 2.2 jet data of Eggers[30]; comparison of centerline velocity decay and velocity profile predictions at $X/r_J = 8$ and 27.

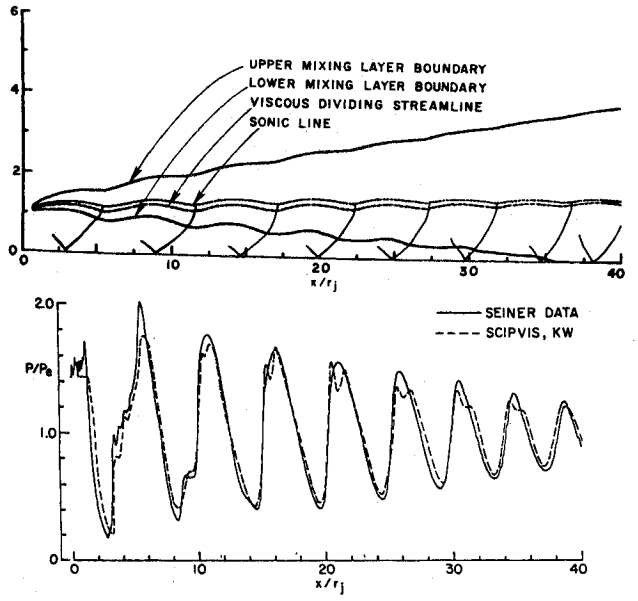

Fig. 7 Predicted flow structure and comparison of predicted and measured centerline pressure variations for a cold, Mach 2 mildly underexpanded jet exhausting into still air.

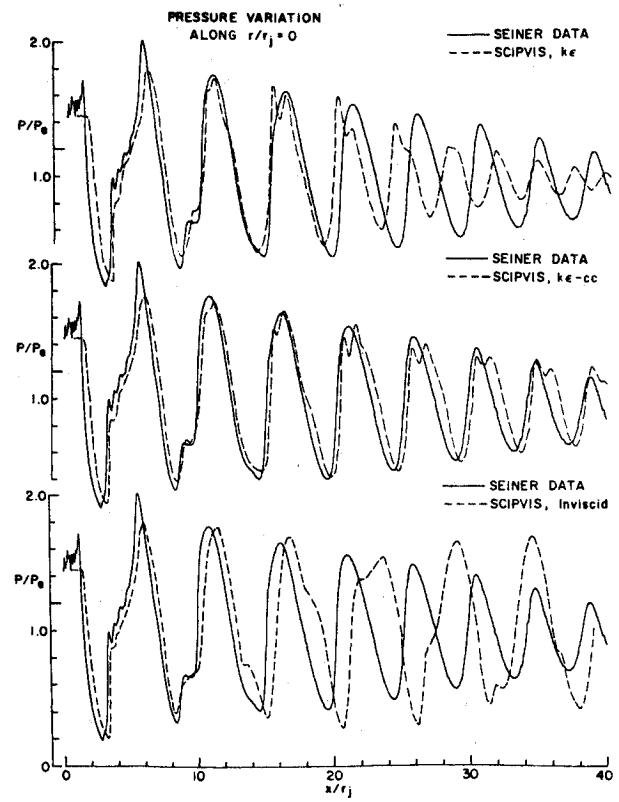

Fig. 8 Comparison of predicted and measured streamwise pressure variations along a jet axis using $k\epsilon$ and $k\epsilon$,*cc* turbulence models, and in inviscid (hyperbolic mode) limit.

V. Jet Flowfield Calculations

The calculations presented here serve to exemplify the overall capabilities of SCIPVIS in analyzing a variety of jet flowfields pertinent to aircraft exhaust problems. Previous papers[3,4,10] have exhibited the ability of the algorithms in SCIPVIS to deal with supersonic interactive phenomena (viz., wave/shear-layer interactions), to treat significantly underexpanded jets exhausting into a supersonic stream simulating conditions encounterable in rocket exhaust plume problems, and to analyze low-speed parabolic mixing problems.

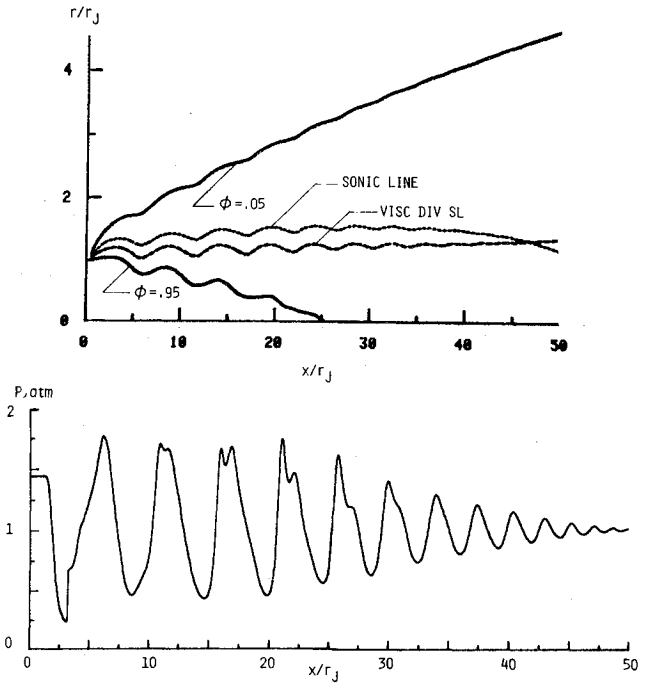

Fig. 9 Predicted flow structure and centerline pressure variation for a hot, Mach 2 mildly underexpanded jet exhausting into still air.

Supersonic Balanced Pressure Jet Mixing

SCIPVIS can perform supersonic balanced pressure jet mixing problems in either a parabolic or fully coupled viscous/inviscid mode. Unless the weak waves induced by the mixing process[3] are of interest, the results using either of these modes are virtually identical. Figure 5 compares a fully coupled SCIPVIS prediction for a balanced pressure Mach 2.2 jet into still air with a parabolic BOAT code[15] prediction. The $k\epsilon 2$ model was implemented for these runs. A prediction made running SCIPVIS in the parabolic mode was virtually identical to the fully coupled prediction except for the wavelets in the core region and, thus, is not exhibited. The wavelets are physical (see the measurements of McLaughlin et al.,[29] in particular Fig. 5 of Ref. 29 which exhibits the measured centerline Mach number variation for a Mach 2 jet into still air) and are generated by the interaction mechanism discussed in Refs. 3 and 4.

The performance of three turbulence models in SCIPVIS (parabolic mode) in predicting the decay in centerline velocity for the Mach 2.2 jet is exhibited in Fig. 6 and compared with the data of Eggers.[30] Velocity profiles at $X/r_J = 8$ and 27 are compared with data in Fig. 6. The comparisons here indicate that the kW turbulence model does the best overall job, the $k\epsilon 2$ model mixes too fast, and the $k\epsilon 2$,*cc* model mixes somewhat too slowly.

Underexpanded Mach 2 Jet, $P_J/P_E = 1.45$

A series of calculations was performed to exhibit the flow characteristics of modestly underexpanded cold ($T_J = 164$ K) and hot ($T_J = 1500$ K) (exit static pressure ratio, $P_J/P_E = 1.45$) Mach 2 jets exhausting into still air and a supersonic external stream. The first calculation simulates the experiment of Seiner and Norum[1,2] for the cold jet into still air. The predicted flow structure for this case (using the kW turbulence model option) is exhibited in Fig. 7 for the first 40 jet radii in which eight shock cells occur. The nominal upper and lower mixing layer boundaries (where $\phi = 0.05$ and 0.95, respectively), the jet mixing layer sonic line, and the viscous dividing streamline (where $\psi = \psi_J$) are all depicted. Note that the mixing layer engulfs the entire jet downstream of $X/r_J \sim 35$. The sonic line initially sits above the viscous dividing streamline, intersects it at $X/r_J \sim 45$, and ultimately reaches the axis.

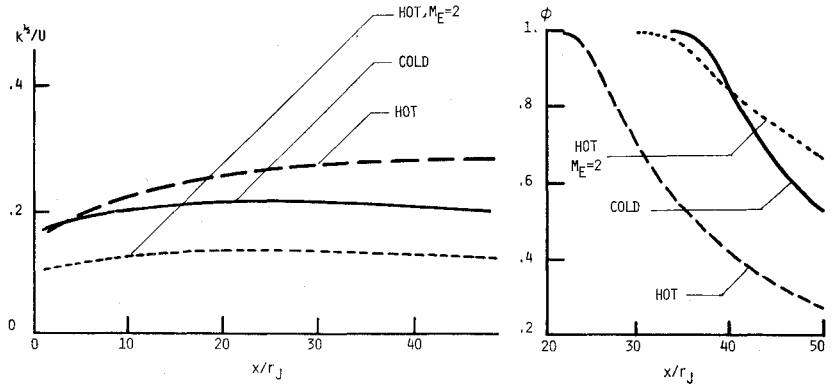

Fig. 10 Comparison of scalar centerline decay rate and peak turbulent intensity levels for cold and hot Mach 2 jets into still air, and hot Mach 2 jet into Mach 2 external stream.

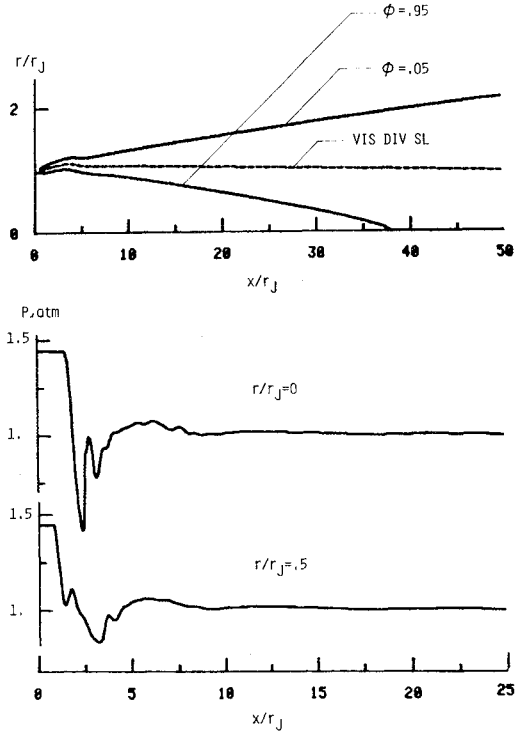

Fig. 11 Predicted flow structure for hot, mildly underexpanded Mach 2 jet into Mach 2 external stream ($U_J/U_E \sim 2.5$), and static pressure variations along jet centerline and off-axis ($r/r_J = 0.5$) position.

The streamwise pressure variations along the jet centerline are compared with measurements[1,2] in Fig. 7; the agreement is quite good indicating that the propagation of the waves through the turbulent mixing layer and the damping of wave strengths due to turbulent dissipation are properly modeled. The marked sensitivity of the wave pattern to the turbulence modeling can be gleaned from the comparisons in Fig. 8. Here, predicted centerline pressure variations using the $k\epsilon$ model, the $k\epsilon$,*cc* model, and in the inviscid limit are compared with data. The $k\epsilon$ model predicts too fast a rate of mixing and, hence, foreshortens the cell lengths and dampens the wave strengths prematurely. The inviscid solution predicts no wave damping or cell foreshortening and a linear solution with constant cell length and wave strength will persist for numerous cells downstream (subject only to numerical damping whose level is quite negligible compared to the physical turbulent levels of the problem). The $k\epsilon$,*cc* model agrees reasonably well with the data and appears to mix somewhat too slowly. The performance of the turbulence models here is in accord with that of the perfectly expanded Mach 2.2 jet comparisons (Fig. 6).

In the second calculation, a hot jet into still air was simulated by boosting the jet total temperature to yield an exit static temperature of 1500 K. Exit pressure and Mach number were kept the same as the cold jet case. The predicted flow structure for this case is exhibited in Fig. 9. The mixing here (using the kW turbulence model) is significantly faster than that in the cold jet case with the mixing layer engulfing the entire jet for $X/r_J > 25$. A comparison of the centerline variation of the species parameter (which for air/air mixing simply represents a tracer species) for the two cases (Fig. 10) clearly exhibits the differences in the mixing rate. The streamwise variation in peak turbulent intensity levels ($k^{\frac{1}{2}}/U$) for the two cases is exhibited in Fig. 10. The hot jet has turbulent levels approximately 30-40% larger than those of the cold jet. The predicted variation of centerline static pressure is exhibited in Fig. 9 and indicates a more rapid decay of peak pressure levels than in the cold jet case.

For the third calculation, the hot jet case was run simulating Mach 2 supersonic flight conditions. The predicted flow structure is exhibited in Fig. 11 where the rate of mixing is seen to be considerably slower than the previous two cases due to the velocity ratio effect (in the previous two cases, the velocity ratio U_J/U_E was essentially infinite; here it is approximately 2.5/1). The significantly slower mixing rates are also evidenced in the species centerline decay (Fig. 10) and the peak turbulent intensity levels (Fig. 10) are seen to be about half of those of the hot jet into still air. Of particular interest here is the *absence* of any noticeable wave structure beyond the first shock cell. In supersonic/supersonic shear-layer interactions,[3] an impinging wave is partially transmitted and reflected in accordance with the structural features of the shear layer (whereas for supersonic/quiescent shear-layer interactions, no transmission occurs and the wave reflects from the sonic line). Under the conditions of this case, the strength of the reflected wave resulting from the interaction at the end of the first shock cell is quite small and thus, the transmitted wave intensity is comparable to that of the impinging wave. This is evidenced in the predicted streamwise pressure variations along the jet axis and along $r/r_J = 0.5$ (Fig. 11) which show no noticeable pressure variations beyond the first shock cell.

Underexpanded Mach 2 Jet, $P_J/P_E = 5$

The hot jet calculations discussed above were repeated with the pressure ratio boosted to 5/1 to exhibit other interesting features of the flow structure. The predicted near-field flow structure is exhibited in Fig. 12 and a Mach disk of significant radius is seen to occur. (In all previous cases, regular reflection occurred.) The jet and Mach disk mixing layers are shaded and shown to intersect at $X/r_J \sim 15$. Note that beyond the Mach disk position, there are two sonic lines in the flow and, for $X/r_J \sim 10$, the code is utilizing *all* of its integration options (i.e., the partially parabolic option below the Mach disk sonic line; the hyperbolic/parabolic option between the Mach disk sonic line and the upper edge of the Mach disk mixing layer, and, between the lower edge of the jet mixing layer and jet sonic line; the hyperbolic option above the two mixing layers;

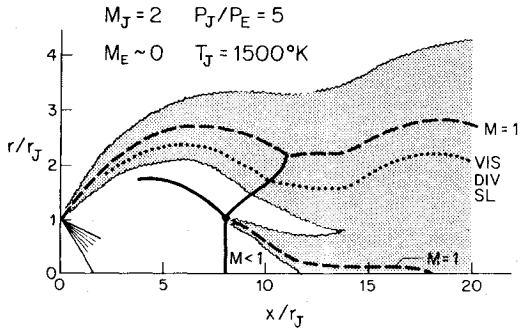

Fig. 12 Predicted near-field flow structure for underexpanded ($P_J/P_E = 5$) hot ($T_J = 1500$ K) Mach 2 jet into still air.

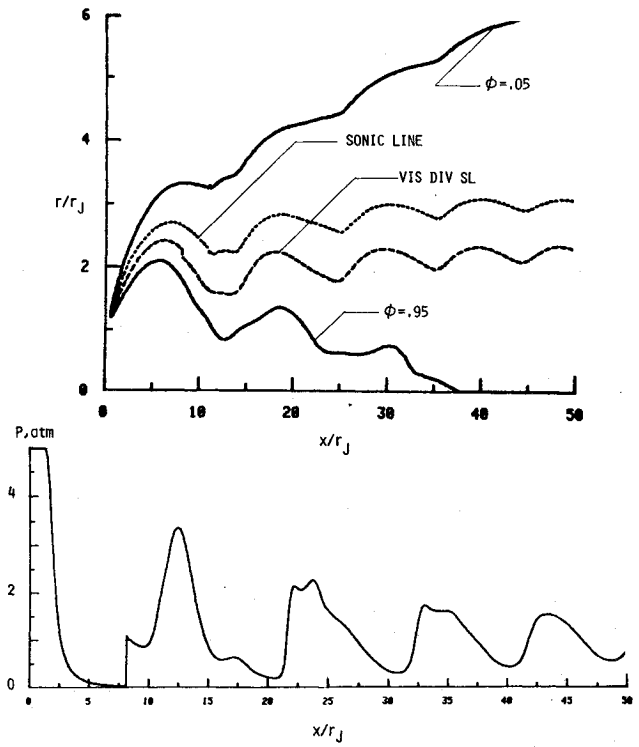

Fig. 13 Predicted flow structure and centerline static pressure variation for a hot, underexpanded Mach 2 jet into still air.

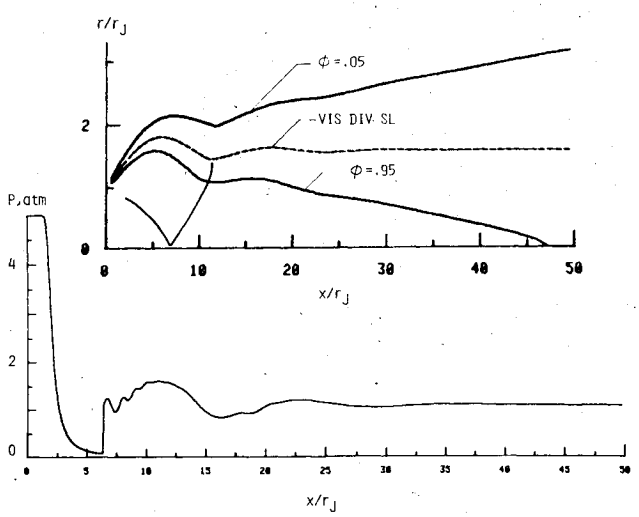

Fig. 14 Predicted flow structure and centerline static pressure variation for a hot, underexpanded Mach 2 jet into Mach 2 external stream.

and, the parabolic option above the jet mixing layer sonic line). The overall flow structure for $0 < X/r_J < 50$ is depicted in Fig. 13 and encompasses about five shock cells. The mixing engulfs the entire plume at $X/r_J \sim 35$-40. The variation of static pressure along the jet centerline is exhibited in Fig. 13.

With a Mach 2 supersonic flight velocity, the features of the flow structure (Fig. 14) change considerably. In particular, no Mach disk occurs, the mixing is considerably slower, and the wave structure is negligible beyond the second shock cell. This is evidenced by the predicted centerline pressure variation exhibited in Fig. 14 where the pressure is seen to be at ambient levels for $X/r_J \sim 30$.

VI. Concluding Remarks

The features and capabilities of the SCIPVIS model for the analysis of turbulent imperfectly expanded jets have been exhibited. The preliminary version is limited to the analysis of axisymmetric or planar jets exhausting into a supersonic or quiescent external stream. A detailed assessment of the model's performance in analyzing laboratory jet data is provided in Part II of this article.

The unique combination of modeling techniques contained in SCIPVIS permits analyzing the detailed multiple-cell jet shock structure in a complex turbulent environment. The interactions between wave processes and the turbulence appear to be adequately modeled via the solution of a fully coupled system of viscous/inviscid equations utilizing a shock-capturing methodology and implementing compressibility modified two-equation turbulence model formulations. Principal uncertainties in the predictions are felt to arise from the probable inability of the turbulence models contained in SCIPVIS to represent the turbulence structure accurately over the full range of conditions of interest and the present inability to account for the induced accelerative effects of jet entrainment for quiescent external streams. Both of these items are now being addressed. The turbulence models are being assessed using the new body of supersonic turbulent jet data gathered at Calspan[31] and deficiencies are being remedied using a new hybrid formulation.[32] A potential and/or panel flow solver is being coupled with SCIPVIS to predict the effects of jet entrainment on the external stream. The coupling will also permit analyzing subsonic/transonic external streams using several iterative sweeps of the jet and potential flow solutions.

Acknowledgment

The work reported herein was supported by NASA Langley Research Center under Contract NAS1-16535.

References

[1]Seiner, J. M. and Norum, T. D., "Experiments of Shock Associated Noise on Supersonic Jets," AIAA Paper 79-1526, 1979.

[2]Seiner, J. M. and Norum, T. D., "Aerodynamic Aspects of Shock Containing Jet Plumes," AIAA Paper 80-0965, 1980.

[3]Dash, S. M. and Wolf, D. E., "Interactive Phenomena in Supersonic Jet Mixing Problems, Part I: Phenomenology and Numerical Modeling Techniques," *AIAA Journal*, Vol. 22, July 1984, pp. 905-913.

[4]Dash, S. M. and Wolf, D. E., "Interactive Phenomena in Supersonic Jet Mixing Problems, Part II: Numerical Studies," *AIAA Journal*, Vol. 22, Oct. 1984, pp. 1395-1404.

[5]Dash, S. M., Pergament, H. S., and Wolf, D. E., "Computation of Viscous/Inviscid Interactions in Exhaust Plume Flowfields, Part I: Overlaid and Fully-Coupled Methodology," *Symposium on Rocket/Plume Fluid Dynamic Interactions, Vol. I—Base Flows*, Univ. of Texas Fluid Dynamics Lab. Rept. 83-101, Austin, Texas.

[6]Dash, S. M., "Computational Techniques for the Viscous/Inviscid Analysis of Exhaust Plume Flowfields," *Advances in Computer Methods for Partial Differential Equations IV*, edited by R. Vichnevetsky and R.S. Stepleman, Int. Assoc. for Math. and Computers in Simulation, Rutgers Univ., New Brunswick, N.J., 1981.

[7]Dash, S. M. and Pergament, H. S., "A Computational System for the Analysis of Mixing/Chemical/Shock Processes in Supersonic Internal and Exhaust Plume Flowfields," AIAA Paper 80-1255, 1980.

[8]Dash, S. M., Pergament, H. S., and Thorpe, R. D., "Computational Models for the Viscous/Inviscid Analysis of Jet Aircraft Exhaust Plumes," NASA CR-3289, 1980.

[9]Dash, S. M. and Thorpe, R. D., "Shock-Capturing Model for One- and Two-Phase Supersonic Exhaust Flow," *AIAA Journal*, Vol. 18, July 1981, pp. 842-851.

[10]Dash, S. M. and Wolf, D.E., "Fully-Coupled Analysis of Jet Mixing Problems, Part I: Shock-Capturing Model, SCIPVIS," NASA CR in preparation.

[11]Pergament, H. S., "Assessment and Recommendation of Two-Equation Turbulence Models for Rocket and Aircraft Plume Flowfield Predictions," NWC TP 6364, July 1982; also, *JANNAF 13th Plume Technology Meeting*, CPIA Pub. 357, Vol. I, April 1982, pp. 115-182.

[12]Launder, B. E., Morse, A., Spalding, D. B., and Rodi, W., "Prediction of Free Shear Flows: A Comparison of Six Turbulence Models," *Free Turbulent Shear Flows*, Vol. 1, NASA SP 321, 1972, pp. 361-426.

[13]Dash, S. M., Weilerstein, G., and Vaglio-Laurin, R., "Compressibility Effects in Free Turbulent Shear Flows," AFOSR-TR-75-1436, Aug. 1975.

[14]Wilmoth, R. G. and Dash, S. M., "A Viscous-Inviscid Interaction Model of Jet Entrainment," *Computation of Viscous-Inviscid Interactions*, AGARD CP 291, 1981, pp. 13.1-13.15.

[15]Dash, S. M., Wilmoth, R. G., and Pergament, H. S., "An Overlaid Viscous/Inviscid Model for the Prediction of Nearfield Jet Entrainment," *AIAA Journal*, Vol. 16, Sept. 1979, pp. 950-958.

[16]Ferri, A. and Dash, S. M., "Viscous Flow at High Mach Numbers with Pressure Gradients," *Viscous Interaction Phenomena in Supersonic and Hypersonic Flow*, University of Dayton Press, Dayton, Ohio, 1970, pp. 271-318.

[17]Patankar, S. V. and Spalding, D. B., "A Calculational Procedure for Heat, Mass, and Momentum Transfer in Three-Dimensional Parabolic Flows," *International Journal of Heat and Mass Transfer*, Vol. 15, Oct. 1972, pp. 1787-1806.

[18]Launder, B. and Spalding, D. B., *Lectures in Mathematical Models of Turbulence*, Academic Press, London, 1972.

[19]Spalding, D. B., "Concentration Fluctuations in a Round Turbulent Free Jet," *Chemical Engineering Science*, Vol. 26, 1971, pp. 95-107.

[20]Saffman, P. G., "A Model for Inhomogeneous Turbulent Flow," *Proceedings of the Royal Society*, Ser. A317, 1970, p. 417.

[21]Millinazzo, F. and Saffman, P. G., "Turbulence Predictions for the Inhomogeneous Mixing Layer," *Studies in Applied Mathematics*, Vol. 55, 1976, pp. 45-63.

[22]Walker, B. J., "Turbulence Model Comparisons for Shear Layers and Axisymmetric Jets," USAMC TR RD-80-1, 1980.

[23]Birch, S. F. and Eggers, J. M., "A Critical Review of the Experimental Data for Developed Free Turbulent Shear Layers," *Free Turbulent Shear Flows Conference Proceedings*, NASA SP-321, 1973, pp. 11-40.

[24]Launder, B. E. and Spalding, D. B., "The Numerical Computation of Turbulent Flows," *Computer Methods in Applied Mechanics and Engineering*, Vol. 3, 1974, pp. 269-289.

[25]Jensen, D. E. and Wilson, A. S., "Prediction of Rocket Exhaust Flame Properties," *Combustion and Flame*, Vol. 25, 1975, pp. 43-55.

[26]Nelius, M. A., Darlington, C. R., and Wasson, R. A., "Exhaust Plume Gas Dynamic and Radiation Measurements on a 500 lbf Thrust Liquid Rocket Engine at Simulated Flight Conditions," AEDC-TR-77-44, July 1977.

[27]Dash, S. M. and Sinha, N., "Noniterative Cross-Flow Integration for the Pressure-Split Analysis of Subsonic Mixing Layer Problems," *AIAA Journal*, Vol. 23, Jan. 1985, pp. 153-155.

[28]MacCormack, R. W., "The Effects of Viscosity in Hypervelocity Impact Cratering," AIAA Paper 69-354, 1969.

[29]McLaughlin, D. K., Seiner, J. M., and Liu, C. H., "On the Noise Generated by Large Scale Instabilities in Supersonic Jets," AIAA Paper 80-0964, 1980.

[30]Eggers, J. M., "Velocity Profiles and Eddy Viscosity Distributions Downstream of a Mach 2.2 Nozzle Exhausting to Quiescent Air," NASA TN D-3601, 1966.

[31]Padova, C. and Boyer, D. W., "Mach Number and Density Effects in the Mixing of Supersonic Jets," *JANNAF 14th Plume Technology Meeting*, CPIA Pub. 384, Vol. I, 1983, pp. 107-116.

[32]Pergament, H. S., Sinha, N., and Dash, S. M., "Hybrid Two-Equation Turbulence Model for Supersonic Free Shear Layers and Jets," Science Applications Inc., Princeton, N.J., TM-26, Sept. 1984.